The avalanche-mode superjunction LED

Dutta, S.; Steeneken, Peter; Agarwal, V.; Schmitz, J.; Annema, A.-J.; Hueting, R.J.E.

DOI
10.1109/TED.2017.2669645

Publication date
2017

Document Version
Accepted author manuscript

Published in
IEEE Transactions on Electron Devices

The Avalanche Mode Superjunction Light-emitting Diode

S. Dutta, *Student Member IEEE*, P.G. Steeneken, V. Agarwal, J. Schmitz, *Senior Member IEEE*, A.J. Annema, and R.J.E. Hueting, *Senior Member IEEE*.

***Abstract*—Avalanche-mode light-emitting diodes (AMLEDs) in silicon (Si) are potential light sources to enable monolithic optical links in standard CMOS technology, due to the large overlap of their electro-luminescent (EL) spectra with the responsivity of Si photo-diodes. These EL spectra depend on the reverse electric field. We present, for the first time, AMLEDs employing the superjunction (SJ) assisted reduced surface field (RESURF) effect which increases the uniformity of their electric field profile. Consequently, the EL area of these lateral devices is significantly enlarged as compared to conventional AMLEDs. Electrical and optical measurements demonstrate RESURF, as predicted by TCAD simulations, and show a direct link between EL-intensity (optical power per unit device area) and the field-profile. Contrary to a conventional AMLED, the breakdown voltage of the SJ-LED scales with the device length. Further, the brightest SJ-LED, with a lateral intensity of $\sim$30 mW cm^{-2} at an electrical power (P_{AMLED}) of 0.1 W, shows a 2-fold higher internal quantum efficiency and a 3-fold higher EL-intensity compared to the conventional AMLED for the same P_{AMLED}.**

***Index Terms*—avalanche breakdown, RESURF, silicon, electro-luminescence, LED, photo-diode, internal quantum efficiency.**

I. Introduction

The avalanche-mode light-emitting diode (AMLED) is a potential candidate as a silicon (Si) based light source in high speed monolithic optical links in standard Complementary Metal-Oxide-Semiconductor (CMOS) technology [1]–[7]. This is primarily due to two features. Firstly, the electro-luminescent (EL) spectra of AMLEDs have a significant overlap with the spectral responsivity of Si photo-diodes, as compared to that of forward biased LEDs. Secondly, AMLEDs can be modulated at high speeds ($\sim$ 20 GHz) [8], which is governed by the short carrier transit time ($\sim$ 10 ps) across the depletion region via electric field-assisted drift. In contrast, switching speed of forward biased LEDs is limited by their intrinsic RC-delay and the reverse recovery time [9]. Values in the order of 1 MHz was reported in silicon-on-insulator (SOI) LEDs [9]. The electro-luminescence in avalanche-mode (AM-EL) is governed by impact ionization [10] and hence, by the reverse electric field F [11]. The main challenge, however, has been the relatively lower radiative efficiency of AMLEDs ($\sim 10^{-5}$) [3] as compared to that of forward biased LEDs ($\sim 10^{-3}$) [12], which can be compensated by integrating them with single photon avalanche diodes (SPADs) [13] as detectors, which are sensitive to a few photons. Nevertheless, higher optical emission intensities are desired in AMLEDs because the attainable bandwidth of optical links is critically dependent on the EL-intensity of the LED [14]. Recently, enhanced avalanche-mode light emission has been demonstrated through enhanced injection (current density) [3], [15], carrier momentum and carrier energy engineering [14] with reported intensities up to 200 nW μm^{-2}.

In this work, we propose a new way to improve the spatial uniformity of F and consequently the internal quantum efficiency (IQE) of the LED in a standard 140 nm silicon-on-insulator (SOI)-CMOS technology [16]. This is achieved using the superjunction (SJ) assisted reduced surface-field (RESURF) concept [17]–[20]. Although the SJ concept has been used in Si power devices [21]–[23] to overcome the breakdown voltage (V_{BR}) versus on-resistance (R_{ON}) trade-off, it has not been used in light-emitting diodes (LEDs). The proposed avalanche-mode SJ-LEDs are lateral multi-finger diodes. We show that 1) RESURF is obtained in a standard SOI technology, where V_{BR} can be tuned by the designer via device scaling; 2) a uniform electric field-profile directly translates into uniform AM-EL over the device area (A); 3) the EL-intensity (optical power per unit area) increases with increasing field-uniformity; 4) a higher IQE and a higher EL-intensity can be achieved with the SJ-LED for the same electrical power (P_{AMLED}) as compared to a conventional AMLED.

The rest of the paper is organized as follows. Section II describes the theoretical background and the structural design of the SJ-LEDs. Section III discusses the electrical and optical behavior of the SJ-LEDs along with an implementation example of a monolithic lateral optical link designed in the same technology. Section IV summarizes our conclusions. Section V contains an additional insight into the EL spectra of the SJ-LEDs.

II. Theory and Design of Device

A. Background

Fig. 1 (a) shows the schematic top-view and the sketch of the triangular field-profile $F(x)$ of an abrupt, symmetric p-n junction [24]. The superjunction diode consists of alternate p-

Manuscript changed November 4, 2016.
This work is partly supported by the Dutch Technology Foundation STW, an applied science division of NWO. The authors would like to thank S.M. Smits and J.P. Korterik from MESA+ Institute for Nanotechnology, for experimental support and Maarten Swanenberg from NXP Semiconductors for his valuable suggestions.
S. Dutta, J. Schmitz and R.J.E. Hueting are with the MESA+ Institute for Nanotechnology, University of Twente, 7500AE, Enschede, The Netherlands (e-mail: s.dutta@utwente.nl).
V. Agarwal and A.J. Annema are with the CTIT Institute, University of Twente, Enschede, The Netherlands.
P.G. Steeneken is with NXP Semiconductors, Eindhoven 5656AE, The Netherlands and with Delft University of Technology, Delft 2628CN, The Netherlands (e-mail: peter.steeneken@nxp.com).

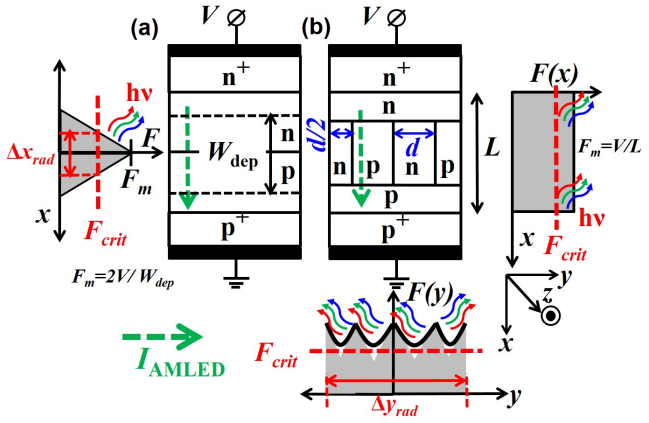

Fig. 1. Schematic top-view of device and field profiles for (a) an abrupt symmetric p-n junction, and (b) a 2D superjunction diode, which increases the uniformity of the magnitude of $F(x,y)$. Light is emitted from (x,y) only if $|F(x,y)|$ exceeds the critical field $F_{\rm crit}$, as indicated by the regions $\Delta x_{\rm rad}$ and $\Delta y_{\rm rad}$. The direction of current $I_{\rm AMLED}$ flow is indicated by the green dashed arrows.

and n-doped fingers as shown in Fig. 1 (b). Optimal RESURF is obtained when the charge in the p-type and n-type fingers is balanced [19]:

$$q \cdot d_{\rm D} \cdot N_{\rm D} + (-q) \cdot d_{\rm A} \cdot N_{\rm A} = 0, \tag{1}$$

where q is the elementary charge, d is the finger width, N is the doping concentration, and the subscripts A and D represent acceptor and donor species respectively. To simplify the design procedure, we choose a symmetric SJ with $N_{\rm A}$=$N_{\rm D}$=N, and thereby equal finger widths $d_{\rm A}$=$d_{\rm D}$=d to satisfy eq. 1. Moreover, a more uniform field-profile is obtained when the fingers are fully depleted along the y-axis at a reverse bias $V < V_{\rm BR}$, where $V_{\rm BR}$ is the avalanche breakdown voltage. This leads to a profile $F(y)$. The fingers at the edges are terminated at a width of $0.5d$, to ensure charge balance and symmetry. At full depletion, the following condition holds:

$$W_{\rm dep} = \sqrt{\frac{4 \cdot \varepsilon_{\rm Si} \cdot V}{qN}} = d, \tag{2}$$

where $W_{\rm dep}$ is the depletion width, and $\varepsilon_{\rm Si}$ is the silicon permittivity.

It is well-known that avalanche breakdown initiates via impact ionization, that accelerates the electron-hole pairs to energies in excess of the band-gap. Upon transition to the valence band, certain fraction of these high energy electrons emit photons, a process described [10], [11] as avalanche-mode electroluminescence (AM-EL). Further, AM-EL is isotropic and occurs from a point (x,y) if $|F(x,y)|$ exceeds the critical field $F_{\rm crit}$. In silicon, the EL-spectra has been shown to peak in the visible range which is attractive from the point-of-view of efficient detection via Si photo-diodes owing to the large overlap with their spectral responsivity. In particular, SPAD based detectors in Si, which are sensitive to the photon-count can offer high speed optical data communication [13] if the IQE of the LEDs can be enhanced for a given device area. This is the objective of this work.

B. Design

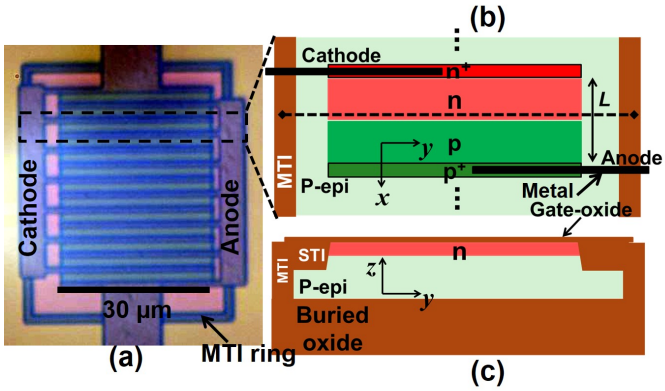

Fig. 2. (a) Die micrograph of D1, (b) blow-up of the top-view of a single diode segment showing a symmetric p-n junction, and (c) the vertical cross-section.

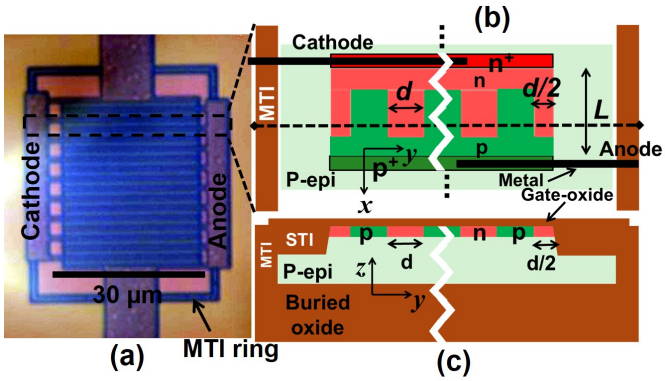

Fig. 3. (a) Die micrograph of D4, (b) blow-up of the top-view of a single diode segment showing the symmetric p-n finger pairs terminating at a width of $0.5d$ on both ends of the y-axis, and (c) the vertical cross-section.

Lateral conventional p-n diodes D1 and D3 have been designed as reference devices. Superjunction diodes D2, D4, D5 and D6 are designed with parameters as listed in Table I. For diode D1, Fig. 2 (a) shows the die-micrograph, (b) shows a blown-up schematic top view, and (c) shows the vertical cross-section. The diode consists of symmetric p- and n-type doped layers with an implant dose of 5×10^{12} cm^{-2} that penetrate to a depth of $\sim$0.25 μm into a 1.5 μm thick p-type ($\sim10^{15}$ cm^{-3}) epitaxial Si substrate. This results in an effective doping mean doping N of $\approx 2\times10^{17}$ cm^{-3} in the p- and n-layers. A medium trench isolation (MTI) encloses the device, which along with the buried oxide (BOX) layer, provides galvanic isolation from neighboring devices. The handle wafer beneath the BOX layer is not shown for clarity. Fig. 3 shows the same for the SJ-LEDs. The n$^+$ and p$^+$ regions are separated by a length L, and are separated from the SJ region by an n and p layer respectively, in order to prevent the formation and premature breakdown of n$^+$p or p$^+$n junctions. In the

TABLE I
LIST OF TEST-DEVICES SHOWING GEOMETRICAL DESIGN PARAMETERS, BREAKDOWN VOLTAGES AND VARIANCE ACROSS DIFFERENT DIES.

Device	L (μm)	d (μm)	Area: A (μm^2)	V_{BR} (V): Measured [TCAD]	Die variance (%)
D1 (pn)	2	–	780	29.0 [30.1]	3.6
D2 (pn)	2	0.384	780	50.0 [49.0]	3.9
D3 (pn)	1	–	510	25.8 [26.0]	2.2
D4 (pn)	1	0.384	510	28.4 [29.2]	2.6
D5 (pn)	1	0.576	510	27.6 [28.7]	4.8
D6 (pn)	1	0.768	510	26.6 [26.3]	1.8

SJ-LEDs namely, D2, D4, D5 and D6, d and L have been varied as listed in Table I. The shallow SJ implants provide low attenuation for the vertically emerging light. Further, silicide protection masks are used on the entire active area except the electrodes to facilitate the off-chip vertical measurement of the EL-spectra via a spectrometer. Light can also be detected on-chip via integrated photo-diodes, which will be discussed later in section III-B.

III. ANALYSIS AND RESULTS

A. Electrical characteristics

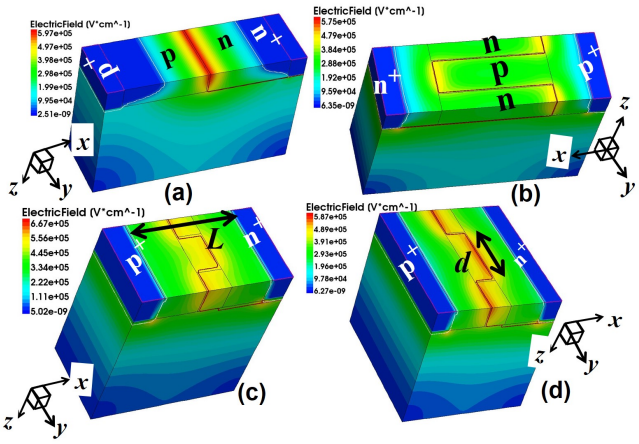

Fig. 4. TCAD simulated field profiles $|F(x,y,z)|$ for (a) D1 at V=35 V, showing a peak field at the junction (similar to D3 with L=1 μm), (b) D2 at V=52 V: SJ diode with L=2μm and d=0.384 μm, showing RESURF, (c) D4 at V=40 V with L=1μm and d=0.384 μm, and (d) D6 at V=35 V with L=1μm and d=0.768 μm. Similar profiles are obtained for D5 and D6, hence D5 is omitted for brevity. The coordinate axes are shown for each device separately for clarity.

Fig. 4 shows the TCAD [25] simulated 3-D field profiles of the designs, while Figs. 5, and 6 show the profiles along x and y axis respectively. The peak field F_m is at the junction in a conventional p-n diode (Fig. 4 (a)), while in an SJ-diode, with suitably chosen d and L [26], for a given V, the fingers deplete along y faster than along x, leading to full depletion (Fig. 4 (b)), obtained for L=2 μm and d=0.384 μm. Charge balance results in field peaking at the opposite

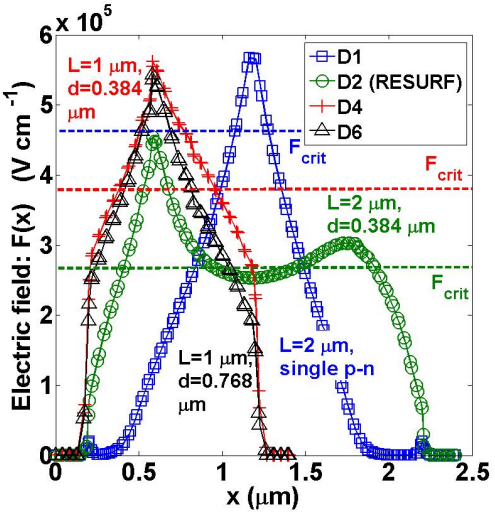

Fig. 5. TCAD simulated field profiles $F(x)$ at V=35 V for D1 (blue), showing a peak field at the junction, at V=52 V for D2 (green), where full depletion is obtained. In D4 (red) and D6 (black), as d reduces, $F(x)$ becomes more uniform. The p^+ edge is at x=0. The respective F_{crit} values are indicated with the dashed lines.

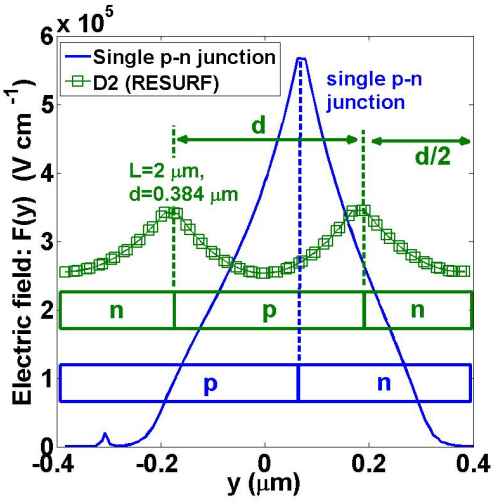

Fig. 6. TCAD simulated field profiles $F(y)$ at V=52 V for D2 (green), showing its hyperbolic shape and more uniformity as compared to a single p-n junction (blue) of a similar size (as a guide to the eye) at a suitable V. Pinch-off of the depletion regions in the fingers (eq. (2)) occurs at $V < V_{BR}$.

corners [26] of the p and n fingers. The spread in the field profile increases the width of the region where $F(x,y) > F_{crit}$, thereby increasing the width of the EL-region in avalanche breakdown. The TCAD simulated values of F_{crit} are indicated also in Fig. 5. Full depletion along y also increases the spatial field-uniformity as shown in Fig. 6. For a given L, as d reduces, $F(y)$ becomes more uniform and spreads more as shown in Figs. 4 (c), (d), 5 and 7. Full depletion of the fingers along y in D2 occurs at a bias $V \approx 5$ V when condition (2) is satisfied. This leads to a sharp drop in the measured capacitance C [28] as observed from the measured C-V characteristics in Fig. 8. Thus, less charge removal is needed for a fixed change in C in D2 as compared to D1. The zero bias capacitance $C(V=0)$ is about 2.5 times higher in

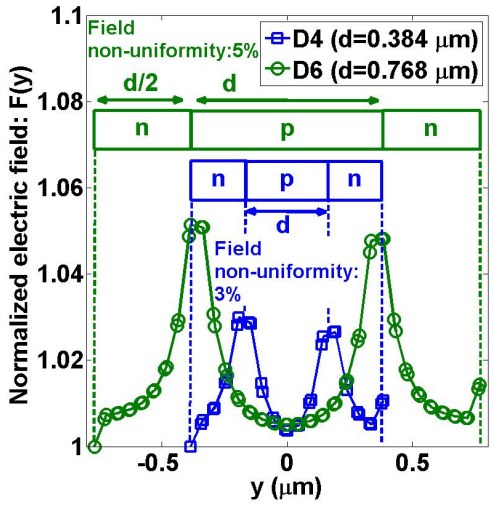

Fig. 7. TCAD simulated field profiles $F(y)$ at V=40 V for D4 (blue), and at V=35 V for D6 (green). Values are normalized w.r.t. the individual minimum $F(y)$ for comparison. As d reduces for a fixed L, the field "non-uniformity" reduces.

D2 than in D1 owing to a higher number of junctions ($\approx$ 25) for the same device area A. As a visual example, the TCAD simulated 2-D field profiles for the SJ-LED D2 are shown in the insets at V=2 V, where there is partial depletion, and at V=20 V, where there is full depletion.

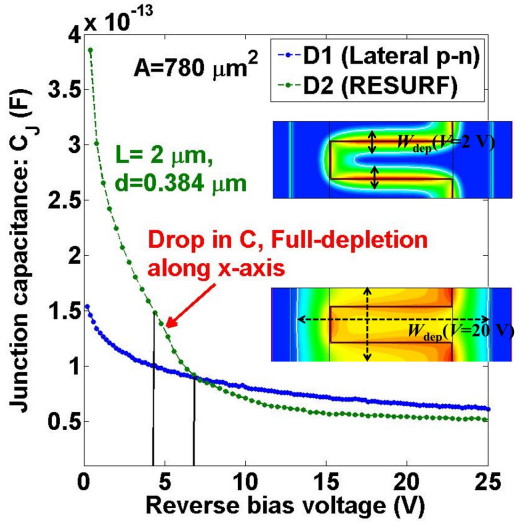

Fig. 8. Measured reverse C-V characteristics of D1 (blue) and D2 (green). The full depletion along y-axis due to RESURF leads to a sharp drop in C [28]. This occurs when condition (2) is satisfied. The insets show the TCAD simulated 2-D view of the field profile $F(x,y)$ of D2 at V=2 V (partial depletion) and V=20 V (full depletion).

RESURF also leads to a change in the V_{BR} of the devices. Fig. 9 shows the TCAD simulated versus measured I-V characteristics of D1 and SJ-LED D2 at 300 K, showing a good agreement in the V_{BR}, which has been defined [27] at I=1 μA. With more RESURF in D2, V_{BR} is higher than in D1, while both have the same doping levels and device area. A V_{BR} of about 50 V is also in agreement with the 2-D analytical model in [26] with L= 2 μm and d=0.384 μm. The reverse leakage current is higher in D1 than in D2 (with RESURF), which can be explained by a lower effective carrier lifetime ($\sim$0.1 μs) in D1 than in D2 ($\sim$10 μs). This is possibly due to the different edge termination of the p-n junction in D1, where the shallow trench isolation (STI) layer directly interfaces the junction along the x-axis leading to a higher chance of trap-assisted recombination.

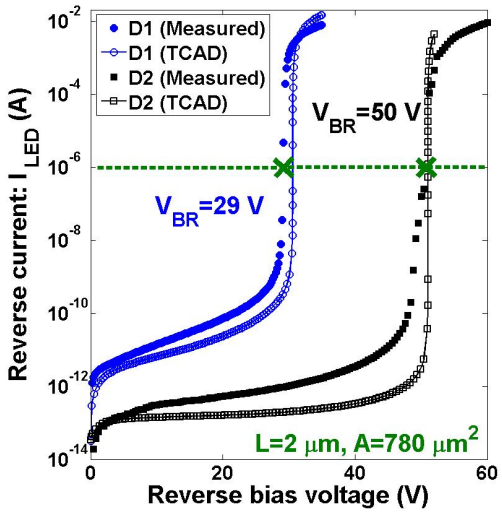

Fig. 9. TCAD simulated and measured reverse I-V characteristics of D1 and SJ-LED D2 at 300 K. Measurement is done using a Keithley 4200 SCS. V_{BR} has been defined [27] at I=1 μA.

Fig. 10 compares the measured with TCAD simulated V_{BR} for D2 to D6. For d=0.384 μm, as L is halved from 2 μm in D2 to 1 μm in D4, V_{BR} also reduces nearly by a factor of 2. An increase in measured V_{BR} is also observed as d reduces for a given L=1 μm, as observed in diodes D3 to D6, due to increasing field uniformity. This trend is also in agreement with the analytical model in [26]. Note that in all diodes, a positive temperature coefficient of the measured V_{BR} was observed (shown for some diodes in the inset of Fig. 10), which confirms avalanche breakdown.

B. Electro-luminescent characteristics

The measured AM-EL spectra of D1 and D2 at 300 K for I_{AMLED}=4 mA and 8 mA are shown in Fig. 11, and those of D3, D4 and D6 are shown in Fig. 12. The light is coupled vertically from the die into an optical fiber feeding an ADC-1000-USB spectrometer from Avantes. Emission is observed in the range 400 nm $< \lambda <$870 nm with a peak at $\lambda \approx$ 650 nm, where λ is the free space photon wavelength. The spectra were modeled for conventional single-sided junctions w.r.t. V and F earlier [11], [29]–[31]. Ripples are observed in the spectra, in particular, in the range 600 nm$< \lambda <$800 nm. This is predominantly due to Fabry-Perot interference in the $\sim$10 μm thick inter-metal dielectric present on the top of the devices, which is experimentally verified as described in the Appendix. For the same device area, the EL-intensity is higher in D2 than in D1, due to a higher field uniformity in

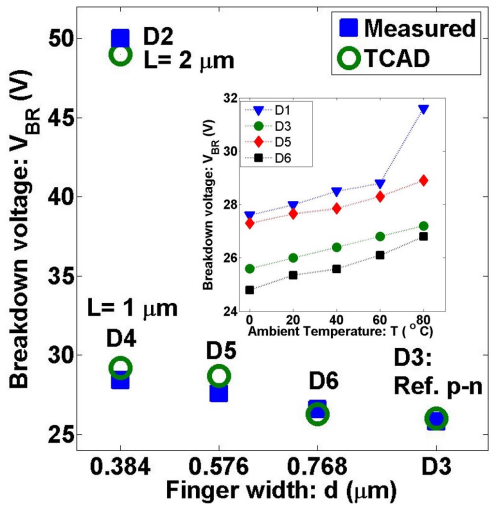

Fig. 10. TCAD simulated and measured V_{BR} for D2 to D6 at 300 K showing good agreement. The trend in V_{BR} is compliant with the one predicted by a 2-D analytical model [26]. (Inset): Measured V_{BR} at different ambient temperatures. Increasing V_{BR} with increasing temperature confirms the avalanche mechanism of breakdown.

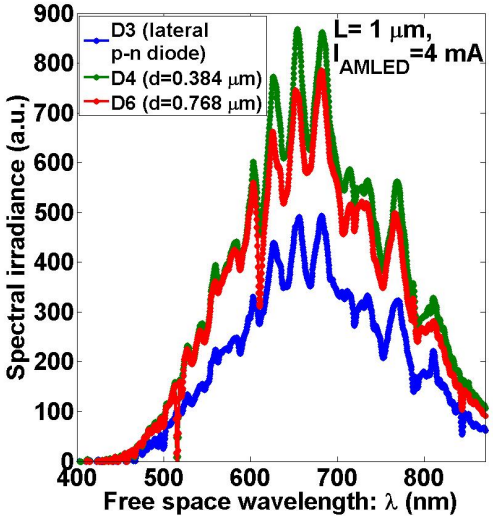

Fig. 12. Measured AM-EL spectral irradiance at 300 K for D3, D4 and D6 at I_{AMLED}=4 mA. The spectra are measured vertically using a 50 μm multi-mode optical fiber feeding an ADC-1000-USB spectrometer from Avantes.

D2. Further, for L=1 μm, as d reduces, a higher uniformity and increased spreading in $F(x,y)$ leads to a higher EL-intensity in D4 as compared to D6.

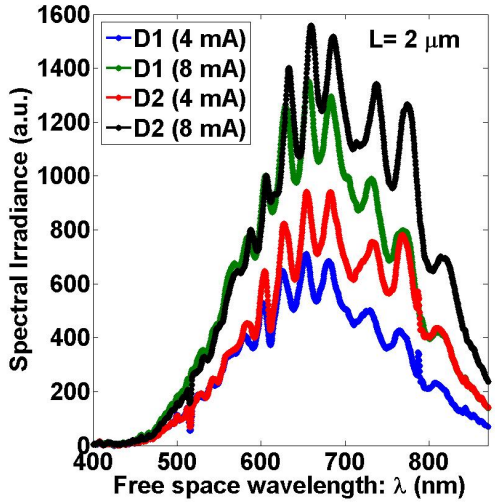

Fig. 11. Measured AM-EL spectral irradiance at 300 K for D1 and D2 at I_{AMLED}=4 mA and 8 mA. The spectra are measured vertically using a 50 μm multi-mode optical fiber feeding an ADC-1000 USB spectrometer from Avantes.

Fig. 13 shows the relative comparison of the AM-EL intensity (optical power per unit device area) w.r.t. electrical power P_{AMLED} for the SJ and reference AMLEDs, evaluated at a fixed I_{AMLED}=4 mA. For L=1 μm, as d is doubled from D4 to D6, a nearly 50 % increase in the EL-intensity is obtained. This also leads to an increase in V_{BR} and thereby P_{AMLED}. Similar reasoning holds for L=2 μm. Further, the EL-intensity of D2 is less than that of D4, which can be explained by the lower value of F_m [11] as seen from TCAD simulated field profile.

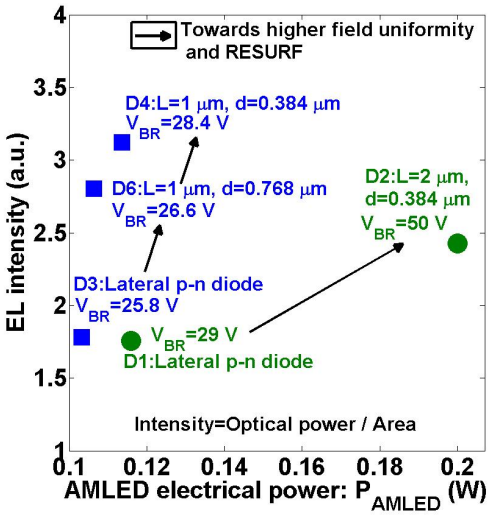

Fig. 13. Relative comparison of AM EL-intensity w.r.t. electrical power for the SJ and reference AMLEDs, at I_{AMLED}=4 mA.

The connection between the spatial uniformity in $F(x,y)$ and AM-electroluminescence is further evident from Figs. 14 (b), (c) and (d). In D2, RESURF leads to a more uniform light emission along the y-axis. The increase in the EL-area implies an increase in the IQE [32] of the SJ-LED. In D6, $F(y)$ is less uniform than in D4 (see also Fig. 7). Under a given optical resolution, the non-uniformity in field results in a discontinuous array of EL-spots in D6. Each spot corresponds to a junction between a p-type and n-type finger.

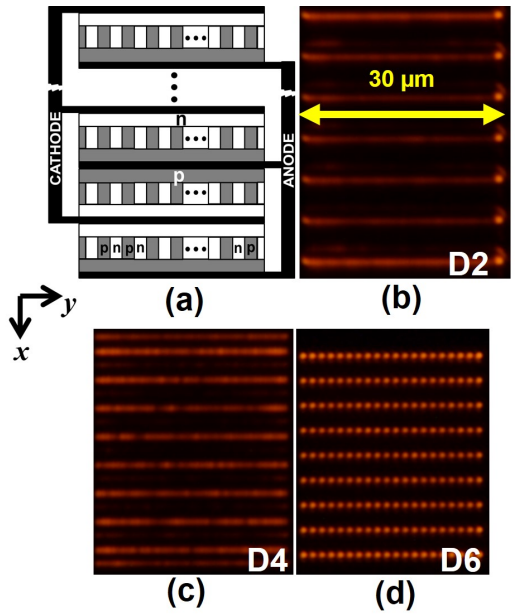

Fig. 14. (a) Schematic top-view of the complete SJ-LEDs showing the location of the fingers and the electrodes. AM-EL micrographs (to the same scale) at a fixed I_{AMLED}=4 mA at 300 K with a visible range camera and an integration time of 25 s are shown for (b) D2, (c) D4 and (d) D6. Light is received along the z axis (vertically). In D6, each discontinuous spot corresponds to a junction between a p-type and n-type finger. Note that the metal lines on the electrodes screen the light.

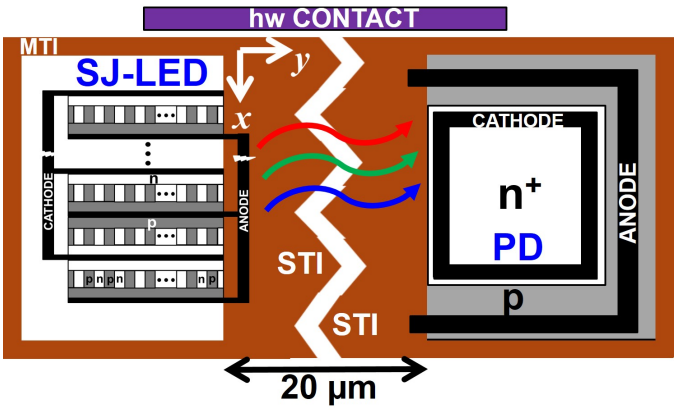

Fig. 15. Schematic top-view of the test optical link used in the measurement. The active areas of D4 and the PD are separated by 20 μm.

C. Implementation in an integrated lateral optical link

Since AM-EL is isotropic, photons can also be detected laterally by an integrated PD (with a limited extraction efficiency η), which is a standard vertical n^+p junction separated from the AMLED by 20 μm along y-axis via a 0.4 μm thick shallow trench isolation (STI) layer as shown in the Fig. 15. The STI layer between the LED and the PD provides a low-attenuation optical path [7]. An electrically insulated vertical poly-Si column serves as a contact between the epitaxial Si and the handle wafer (shown in purple in Fig. 15). This contact provides heat sinking [34] to reduce thermal coupling [7]. A quantitative measure of the brightness of an AMLED in the lateral direction (y-axis) is obtained from the measured I-V characteristics of the PD at various I_{AMLED}, as shown in Fig. 16. The presence of a non-zero short-circuit current I_{SC} and an open-circuit voltage V_{OC} confirms optical coupling [7], [33]. I_{SC} increases proportionally with I_{AMLED} and hence, the incident EL-intensity. Thus, I_{SC} is a measure of the EL-intensity in the given direction. The optical power P_{opt} intercepted by the PD is transduced to photo-voltaic power. The maximum photo-voltaic power delivered to a load is given by the product $I_{\mathrm{SC}} \cdot V_{\mathrm{OC}}$ [33]. Considering that the high internal quantum efficiency of detection of photons in the visible range by a Si PD, we can say that the product $I_{\mathrm{SC}} \cdot V_{\mathrm{OC}}$ is a lower bound estimate of Popt. Subsequently, a quantitative measure for the EL-intensity (I_{opt}) of the LED along y-axis can be defined as:

$$I_{\mathrm{opt}} \approx \frac{P_{\mathrm{opt}}}{A_{\mathrm{SW}} \cdot \eta} = \frac{I_{\mathrm{SC}} \cdot V_{\mathrm{OC}}}{A_{\mathrm{SW}} \cdot \eta}, \tag{3}$$

where A_{SW} is the sidewall area of the EL-region of the AMLED normal to the optical propagation (y-axis), and η is the geometrical extraction efficiency (dimensionless) of the optical link. Subsuming self-absorption in Si, Fresnel reflections at two Si-SiO_2 interfaces, and the solid angle (aperture) subtended by the PD at the AMLED, η is calculated to be $\sim$ 0.4 %.

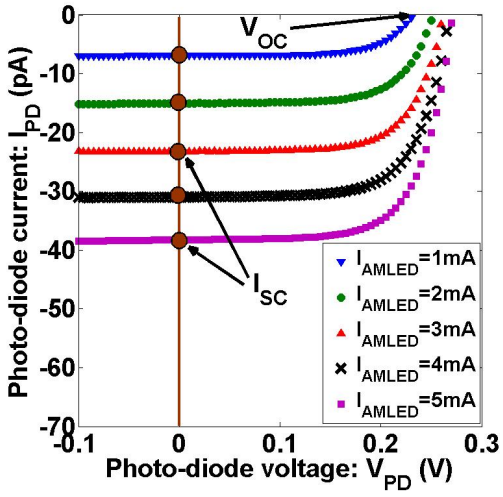

Fig. 16. Measured I-V characteristics of the on-chip PD consisting of a vertical abrupt n^+p junction when illuminated with the avalanche-mode SJ-LED D4 at various I_{AMLED}. Optical generation in the PD junction leads to a non-zero short-circuit current I_{SC} (at V=0). The magnitude of I_{SC} increases with increasing I_{AMLED} and hence EL-intensity.

Using this photo-conductive measurement technique, we can compare the EL-intensity of our brightest SJ-LED D4 with a conventional n^+p AMLED in the same technology. The die micrograph and the EL-micrograph of the conventional AMLED are shown in Fig. 17. The field and consequently EL dominates over the perimeter of the n^+ active area.

Fig. 18 shows the measured I_{SC} of the PD when illuminated by the SJ-LED D4 and a conventional n^+p AMLED in the same technology with a V_{BR} of 16.8 V. Since I_{SC} is proportional to the EL-intensity, therefore the IQE of each LED is proportional to the ratio $I_{\mathrm{SC}}/I_{\mathrm{AMLED}}$. At I_{AMLED}=4

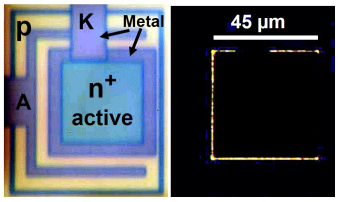

Fig. 17. Top-view (left) and the AM-EL micrograph (right) of the conventional n^+p AMLED at I_{AMLED}=4 mA. The field and hence EL dominated over the perimeter of the n^+ active area.

mA, a 2 times higher IQE is obtained from D4 as compared to the conventional AMLED. Note that the same PD for the same separation is used to detect photons from both the LEDs.

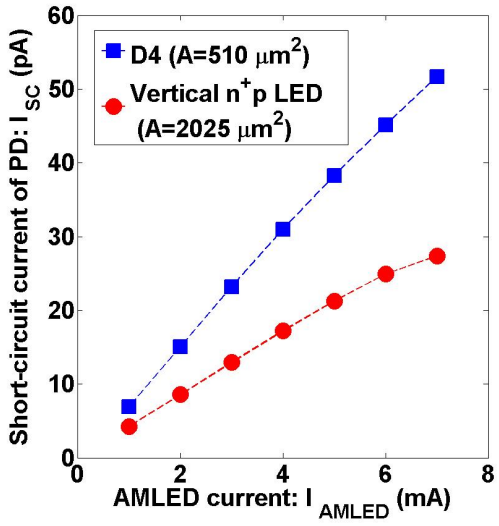

Fig. 18. Comparison of the PD short-circuit current when illuminated by the SJ-LED D4 (blue) and a conventional n^+p AMLED (red) in the same technology with a V_{BR} of 16.8 V, showing a $\approx$ 2 times higher IQE for D4 at a given I_{AMLED}=4 mA.

Fig. 19 compares the AM-EL intensity along y-axis of the SJ-LED D4 with that of the conventional n^+p AMLED versus P_{AMLED}. For the same P_{AMLED}, the EL-intensity of D4 is $\approx$ 3 times higher than that of the conventional AMLED. This is the result of enhancement of the AM-EL region that is linked to the field-profile over the device area.

IV. Conclusions

Avalanche-mode light-emitting diodes employing the superjunction (SJ) assisted reduced surface field effect have been presented for the first time. The devices have been optimized for a higher uniformity in the electric field profile that increases the internal quantum efficiency of avalanche-mode electroluminescence. From spectral measurements, the intensity is shown to increase with increasing field-uniformity. Further, from on-chip photo-conductive measurements of the avalanche-mode superjunction light-emitting diode (SJ-LED) with the highest observed intensity, it is shown that a higher internal quantum efficiency is obtained as compared to a standard avalanche-mode n^+p LED. Further, for the same

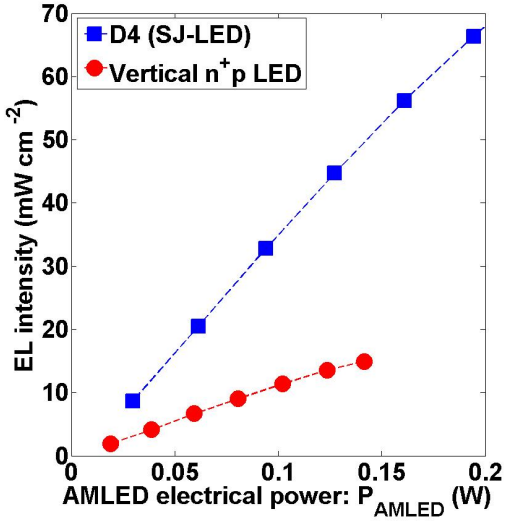

Fig. 19. Comparison of the AM-EL intensity along y-axis of the SJ-LED D4 (blue) and the conventional n^+p AMLED (red) versus P_{AMLED}. For the same P_{AMLED}, the EL-intensity of D4 is $\approx$ 3 times higher than that of the conventional AMLED.

electrical power, the intensity of the particular SJ-LED is 3 times higher than that of the standard n^+p LED. The avalanche-mode SJ-LED is a promising light source for high-speed optical links, when integrated with detectors sensitive to the photon-count (e.g. SPADs).

V. Appendix

The measured AM-EL spectra of our SJ-LEDs exhibit significant ripples, in particular within 600 nm$< \lambda <$800, with local crests and troughs located at specific wavelengths, irrespective of the device under test (DUT). Similar phenomenon was reported earlier [11] in DUTs covered with a thin pure boron layer, but with relatively reduced ripple-amplitudes. In this work, the Si-surface of the SJ-LEDs are covered by a $\sim$10 μm thick multi-layer inter-metal dielectric (back-end). This layer, despite having negligible optical absorption, acts as a composite Fabry-Perot cavity owing to its different refractive index ($\approx$ 1.4) in contrast to that of Si ($\approx$ 4.0). Prior to coupling through the optical fiber, the optical path of the vertically emitted photons consists of the back-end and the 0.25 μm thick Si present between the junction plane and the oxide interface. In order to demonstrate the transmission spectrum of this optical path, we use the principle of reciprocity of light propagation, by operating the DUT (SJ-LED D4) as a PD to transduce light into measurable photo-current.

The optical set-up for this experiment is shown in Fig. 20 is used. Wide-spectrum light from a halogen source is passed through a bifocal convex lens, which creates a parallel beam and filters out IR wavelengths ($\lambda >$900 nm) to reduce heat propagation. The beam is collimated with an entry slit of a monochromator, which is a mirror assembly consisting of a diffraction grating with 1500 lines/mm. The grating creates a spatially resolved continuous line spectrum, which is then

projected onto a mechanically tunable exit slit. The position of the exit slit is then varied to select a specific λ. The position of the 0^{th} order maxima of all colors coincide, thereby producing visible white light at the lowermost position, whose spectrum is shown in Fig. 21. The 1^{st} order maxima follow subsequently, in order of increasing λ. The gap-width of the exit slit can be optimized to allow sufficient intensity to exit, while maintaining a tolerable finesse (sharpness) of the selected spectral line (as desired by the experiment). We use a gap-width of 0.5 mm in this work, and select spectral lines in steps of $\Delta\lambda$=5 nm. The emerging light is subsequently coupled to the optical fiber (the same one is used in measuring the EL-spectra) to illuminate the DUT, operated as a PD. The measured I_{SC} for different λ is proportional to the incident intensity, thereby yielding a relative measure of the transmission spectrum of the optical path as shown in Fig. 21. The positions of the ripples are in good agreement with those obtained in Figs. 11 and 12.

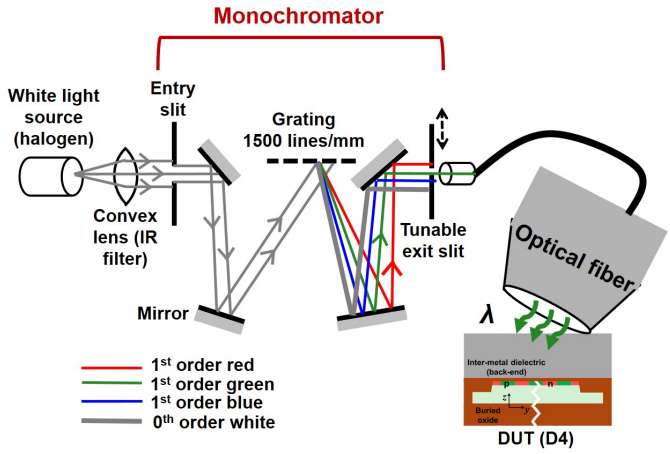

Fig. 20. Schematic of the experimental set-up used to measure the transmission spectrum of the inter-metal dielectric stack covering the SJ-LEDs. The SJ-LED is operated as a photo-diode by illuminating it with light at finely resolved wavelengths ($\approx$ 5 nm). The measured short-circuit current

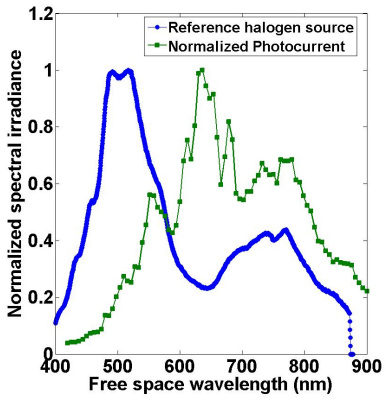

Fig. 21. Normalized spectral irradiance (blue) of the 0^{th} order white light from the monochromator used as an optical source to test the transmission spectrum of the back-end. The normalized photo-current (green) of the test diode is a relative measure of the transmission efficiency around a given optical wavelength.

REFERENCES

[1] B.P. van Drieënhuizen and R.F. Wolffenbuttel, "Optocoupler based on the avalanche light emission in silicon", Sensors and Actuators A, vol. 31, pp. 229-240 (1992).

[2] M. du Plessis, H. Aharoni, and L.W. Snyman, "Silicon LEDs fabricated in standard VLSI technology as components for all silicon monolithic integrated optoelectronic systems", IEEE J. Sel. Topics Quantum Electron., vol. 8, no. 6, pp. 1412-1419 (2002).

[3] L.W. Snyman, M. du Plessis, and H. Aharoni, "Injection-Avalanche-Based n^+pn Silicon Complementary Metal Oxide Semiconductor Light-Emitting Device (450 - 750 nm) with 2-Order-of-Magnitude Increase in Light Emission Intensity", Jpn. J. Appl. Phys., vol. 46, no. 4B, pp. 2474-2480 (2007).

[4] B. Huang, X. Zhang, W. Wang, Z. Dong, N. Guan, Z. Zhang, and H. Chen, "CMOS monolithic optoelectronic integrated circuit for on-chip optical interconnection", Opt. Commun., 284, pp. 3924-3927 (2011).

[5] A. Khanmohammadi, R. Enne, M. Hofbauer, and H. Zimmermann, "Monolithic Integrated Optical Random Pulse Generator in High Voltage CMOS Technology", Proc. 45th ESSDERC, pp. 138-141 (2015).

[6] K. Xu, B. Huang, K.A. Ogudo, L.W. Snyman, H. Chen, and G.P. Li, "Silicon Light-emitting Device in Standard CMOS technology", Proc. 8th International Photonics and OptoElectronics Meetings (2015).

[7] S. Dutta, R.J.E. Hueting, V. Agarwal and A.J. Annema, "An integrated optical link in 140 nm SOI technology", Proc. Conference on Lasers and Electro-Optics, Session JW2A, no. 132 (2016).

[8] A. Chatterjee, B. Bhuva, and R. Schrimpf, "High-speed light Modulation in avalanche breakdown mode for Si diodes", IEEE Electron Device Lett., vol. 25, no. 9, pp. 628-630 (2004).

[9] J. Schmitz, R. de Vries, C. Salm, T. Hoang, R.Hueting and J. Holleman, "On the switching speed of SOI LEDs", Proc. EUROSOI 2008, pp. 101-102.

[10] A.G. Chynoweth and K.G. McKay, "Photon emission from Avalanche Breakdown in Silicon", Phys. Rev., vol. 102, no. 2, pp. 369-376 (1956).

[11] S. Dutta, R.J.E. Hueting, A.J. Annema, L. Qi, L.K. Nanver and J. Schmitz, "Opto-electronic modeling of light emission from avalanche-mode silicon p^+n junctions", J. Appl. Phys., 118, 114506 (2015).

[12] M.A. Green, J. Zhao, A. Wang, P.J. Reece and M. Gal, "Efficient silicon light-emitting diodes", Nature 412, pp. 805-808 (2001).

[13] M. Sergio and E. Charbon, "An intra-chip electro-optical channel based on CMOS single photon detectors", IEEE International Electron Devices Meeting Tech. Digest, Paper no. 822 (2005) (doi: 10.1109/IEDM.2005.1609481).

[14] L.W. Snyman, K. Xu, J-L. Polleux, K.A. Ogudo, and C. Viana, "Higher Intensity SiAvLEDs in an RF Bipolar Process Through Carrier Energy and Carrier Momentum Engineering", IEEE J. Quantum Electron., vol. 51, no. 7, Art. ID 3200110 (2015).

[15] K. Xu, "On the design and optimization of three-terminal light-emitting device in silicon CMOS technology", IEEE J. Sel. Topics Quantum Electron., vol. 20, no. 4, Art. ID 8201208 (2014).

[16] P. Wessels, M. Swanenberg, H. van Zwol, B. Krabbenborg, H. Boezen, M. Berkhout, and A. Grakist, "Advanced BCD technology for automotive, audio and power applications", Solid-State Electronics, vol. 51, 195-211 (2007).

[17] T. Fujihira, "Theory of Semiconductor Superjunction Devices", Jpn. J. Appl. Phys., vol. 36, no.10, part 1, pp. 6254-6262 (1997).

[18] F. Udrea, A. Popescu and W. Milne, "The 3D RESURF junction", in Proc. International Semiconductor Conference, vol. 1, pp. 141-144 (1998).

[19] J.A. Appels, and H.M.J. Vaes, "High Voltage thin layer devices (Resurf devices)", IEDM technical digest, vol. 25, no. 2, pp. 238-241 (1979).

[20] A.W. Ludikhuize, "A Review of RESURF Technology", in Proc. 12th International Symposium on Power Semiconductor Devices, pp. 11-18 (2000).

[21] J. Tihanyi.Power mosfet. U.S. Patent 5 438 215, Aug. 1995.

[22] F. Udrea et al., "3D RESURF double-gate MOSFET: A revolutionary power device concept", Electron. Lett., vol. 34, Issue 8, pp. 808-809 (1998).

[23] M-J. Lin, T-H. Lee, F-L. Chang, C-W. Liaw and H-C. Cheng, "Lateral Superjunction Reduced Surface Field Structure for the Optimization of Breakdown and Conduction Characterisitcs in a High-Voltage Lateral Double Diffused Metal Oxide Field Effect Transistor", Jpn. J. Appl. Phys., vol 42, pp. 7227-7231 (2003).

[24] S.M. Sze and K.K. Ng, "Physics of Semiconductor Devices", 3rd edition, John Wiley & Sons, Inc., USA, 2007.

[25] "Sentaurus TCAD", version L-2016.03, Synopsys Inc.

[26] A.G.M. Strollo, and E. Napoli, “Power superjunction devices: an analytical model for breakdown voltage”, Microelectron. J., 32 (5-6), pp. 491-496 (2001).
[27] Robert F. Pierret, “Semiconductor Device Fundamentals”, Addison-Wesley Publ. (1996).
[28] M. Bobde, L. Guan, A. Bhalla, F. Wang and M. Ho, “Analyzing Superjunction C-V to Estimate Charge Imbalance”, in Proc. 22nd International Symposium on Power Semiconductor Devices, pp. 321-324 (2010).
[29] M. Lahbabi,A. Ahaitouf,M. Fliyou,E. Abarkan,J.-P. Charles, A. Bath, A. Hoffmann, S.E. Kerns and D.V. Kerns, Jr., “Analysis of electroluminescence spectra of silicon and gallium arsenide p-n junctions in avalanche breakdown”, J. Appl. Phys., vol. 95, no.4, pp. 1822-1828 (2004).
[30] N. Akil, S. E. Kerns, D. V. Kerns, Jr., A. Hoffmann, and J. P. Charles, “Photon generation by silicon diodes in avalanche breakdown”, Appl. Phys. Lett., vol. 73, no. 7, 871 (1998).
[31] S. Yamada and M. Kiato, “Recombination Radiation as Possible Mechanism of Light Emission from Reverse-Biased p-n Junctions under Breakdown Condition”, Jpn. J. Appl. Phys., vol. 32, Part 1, no. 10, pp. 4555-4559, 1993.
[32] E.F. Schubert, “Light Emitting Diodes”, Cambridge University Press (2006).
[33] B.G. Streetman, and S.K. Banerjee, “Solid state electronic devices”, 6th ed., Prentice-Hall Inc., ISBN-978-81-203-3020-7.
[34] L. Yan, G. Koops, P. Steeneken, A. Heringa, R. Surdeanu, L. van Dijk, “Integrated heat sinks for SOI power devices”, in Proc. 25th International Symposium on Power Semiconductor Devices, pp. 285-288, 2013 (doi: 10.1109/ISPSD.2013.6694465).